

Supporting Information: Microphase separation in thin films of lamellar forming polydisperse di-block copolymers

Rajeev Kumar,^{*,†,‡} Bradley S. Lokitz,[¶] Scott W. Sides,[§] Jihua Chen,[¶] William T. Heller,^{||} John F. Ankner,^{||} James F. Browning,^{||} S. Michael Kilbey II,[⊥] and Bobby G. Sumpter[¶]

*Computer Science and Mathematics Division, Oak Ridge National Lab, Oak Ridge, TN-37831,
Center for Nanophase Materials Sciences, Oak Ridge National Lab, Oak Ridge, TN-37831,
Center for Nanophase Materials Sciences, Oak Ridge National Laboratory, Oak Ridge, TN-37831,
National Renewable Energy Laboratory, Golden, CO-80401, Spallation Neutron Source, Oak
Ridge National Laboratory, Oak Ridge, TN-37831, and Department of Chemistry, University of
Tennessee, Knoxville, TN-37996*

E-mail: kumarr@ornl.gov

*To whom correspondence should be addressed

[†]Computer Science and Mathematics Division, Oak Ridge National Lab, Oak Ridge, TN-37831

[‡]Center for Nanophase Materials Sciences, Oak Ridge National Lab, Oak Ridge, TN-37831

[¶]Center for Nanophase Materials Sciences, Oak Ridge National Laboratory, Oak Ridge, TN-37831

[§]National Renewable Energy Laboratory, Golden, CO-80401

^{||}Spallation Neutron Source, Oak Ridge National Laboratory, Oak Ridge, TN-37831

[⊥]Department of Chemistry, University of Tennessee, Knoxville, TN-37996

Self-Consistent Field Theory (SCFT) for confined polydisperse di-block copolymers

We consider a melt of n polydisperse di-block copolymer chains in between two parallel substrates. For comparison with neutron reflectivity experiments, one of the walls represents a silicon substrate with a thin layer of silicon oxide (SiO_x) and the other represents a polymer-air interface. We construct the partition function for this particular system by modeling interaction between polymers and substrates by short-range Flory's χ parameter approach.¹ In the following, we consider A-B di-block copolymer chains where the A block is polydisperse and the B is monodisperse.

Representing the copolymer chains by continuous curves ($\vec{R}_\alpha(s)$ for α^{th} chain parameterized by the chain contour variable s containing N_α Kuhn segments), the Hamiltonian for A-B di-block copolymer chains confined between two substrates is written as

$$H = \frac{3}{2l^2} \sum_{\alpha=1}^n \int_0^{N_\alpha} ds \left(\frac{d\vec{R}_\alpha(s)}{ds} \right)^2 + \hat{\rho}_0^{-1} \int d\vec{r} \chi_{AB} \hat{\rho}_A(\vec{r}) \hat{\rho}_B(\vec{r}) \quad (\text{S1})$$

$$+ \hat{\rho}_0^{-1} \int d\vec{r} \sum_{k=s, a, k'=A, B} \chi_{kk'} \rho_k(\vec{r}) \hat{\rho}_{k'}(\vec{r}) \quad (\text{S2})$$

where the first term in H is the chain stretching entropy given by the so-called ‘‘Gaussian thread’’² model for di-block chains with the same Kuhn segment length for each block ($= l$). In this work, we have ignored *inherent* conformational asymmetry between A and B blocks. This is a reasonable approximation for the PGMA and PVDMA-d₆ blocks studied in this work based on our estimates for their Kuhn segment lengths (l_k where $k = \text{PGMA, PVDMA-d}_6$) using approximate relations $l_k^3 \equiv v_k$, v_k being monomeric molar volume. Molar volumes for the GMA and VDMA-d₆ monomers are estimated using group contribution method³ and these estimates are presented in Table S1.

The second and third term in Eq. S2 represent interaction energies between different pairs within Flory-type model, which is parameterized by *dimensionless* χ_{ij} for species of kind i and j . $\hat{\rho}_0 = \sum_{\alpha=1}^n N_\alpha / V$ is the total number density of monomers so that N_α is the polymerization index for chain α and V is the volume containing a finite amount of polymer chains. Later on, $\hat{\rho}_0$ is

Table S1: Estimates of molar volumes of GMA and VDMA-d₆ and Kuhn segment lengths based on group contribution method³

	Monomeric molar volume (v_k) (cm^3/mol)	Kuhn segment length (l_k) (nm)
PGMA	120.68	0.58
PVDMA-d ₆	125.47	0.59

used as a reference density to construct volume fraction profiles from number densities. Using the relation¹ $\chi_{ij}/\hat{\rho}_0 = w_{ij} - (w_{ii} + w_{jj})/2$ and $w_{ii} = 1/(\kappa\hat{\rho}_0^2)$, κ being isothermal compressibility,⁴ it turns out that $\chi_{ij} \sim 1/\hat{\rho}_0$. Similar dependence of χ_{ij} parameter on the reference density (or volume) is postulated in its estimation using solubility parameters.³ Note that reference *mass* density ($\sim \hat{\rho}_0$) can be estimated from neutron reflectivity experiments by preserving stoichiometry while transforming scattering length densities (SLDs) into volume fraction profiles. This is presented in the next section.

In Eq. S2, we have parameterized the interaction energy between the monomers and particles in the substrates by χ parameters. Subscripts a and s are used to represent air and silicon substrate, respectively. For example, χ_{aA} represents the parameter for interaction between A monomer species and the air. Furthermore, regions where polymers interact with substrates are described by functions $\hat{\rho}_k(\vec{r})$ for $k = a, s$, which are taken to be hyperbolic tangent centered at each side of the polymer melt. Such an approach implicitly assumes that the particle density inside the substrates is sufficiently large and continuous density profiles like $\rho_k(\vec{r})$ are appropriate models for the interactions between particles in the substrate and monomers along the polymer chains. Explicitly, the substrate density functions^{5,6} and monomer density operators are written as

$$\rho_s(\vec{r}) = \frac{\hat{\rho}_0}{2} \left[1 - \tanh \left[\frac{z - z_s}{\xi_s} \right] \right] \quad (S3)$$

$$\rho_a(\vec{r}) = \frac{\hat{\rho}_0}{2} \left[1 + \tanh \left[\frac{z - z_a}{\xi_a} \right] \right] \quad (S4)$$

$$\hat{\rho}_A(\vec{r}) = \sum_{\alpha=1}^n \int_0^{N_{\alpha A}} ds \delta(\vec{r} - \vec{R}_\alpha(s)) \quad (S5)$$

$$\hat{\rho}_B(\vec{r}) = \sum_{\alpha=1}^n \int_{N_{\alpha A}}^{N_\alpha} ds \delta(\vec{r} - \vec{R}_\alpha(s)) \quad (S6)$$

where $N_{\alpha A}$ is the number of A monomers in α^{th} chain and z represents the co-ordinate perpendicular to substrates. z_k and ξ_k characterizes the location and width of polymer-substrate interfacial region for $k = s, a$. Also, the choice of so-called masking functions (cf. Eqs. S3- S4) fixes the origin of the coordinate system at the silicon substrate and places the di-block film on the positive z -axis. Note that the SCFT presented here takes the masking functions as an input. For a refined comparison with the neutron reflectivity experiments on the volume fraction profiles in the interior of films, we obtain these functions by *a posteriori* analysis of reflectivity profiles, as detailed in the next section.

The partition function for this system can be written as

$$Z = \int \prod_{\alpha=1}^n D[\vec{R}_\alpha] \exp[-H] \prod_{\mathbf{r}} \delta[\hat{\rho}_0 - \sum_{k=s,a} \rho_k(\vec{r}) - \hat{\rho}_A(\vec{r}) - \hat{\rho}_B(\vec{r})] \quad (S7)$$

The delta function enforces an incompressibility constraint among A monomers, B monomers and the substrates such that the total number density is kept constant. A field theory can be constructed using standard particle to field transformations, which leads to

$$Z = \int D[\rho_A] D[\rho_B] D[\omega_A] D[\omega_B] D[p] e^{-\beta F} \quad (S8)$$

where $\rho_{k=A,B}(\mathbf{r})$ represents collective density variable and $w_{k=A,B}(\mathbf{r})$ is the conjugate field introduced through the exponential representation of the delta functional $\delta[\rho_{k=A,B} - \hat{\rho}_{k=A,B}]$. p is the Lagrange's multiplier which enforces incompressibility constraint. Explicitly, βF , where $\beta = 1/k_B T$ so that k_B is the Boltzmann constant and T is the temperature, is given by

$$\begin{aligned} \beta F = \int d\vec{r} & \left[\hat{\rho}_0^{-1} (\chi_{AB} \rho_A(\mathbf{r}) \rho_B(\mathbf{r}) + \sum_{k=s,a} \sum_{k'=A,B} \chi_{kk'} \rho_k(\mathbf{r}) \rho_{k'}(\mathbf{r})) - i w_A(\mathbf{r}) \rho_A(\mathbf{r}) - i w_B(\mathbf{r}) \rho_B(\mathbf{r}) \right. \\ & \left. - i p(\mathbf{r}) (\rho_0 - \sum_{k=s,a} \rho_k(\mathbf{r}) - \rho_A(\mathbf{r}) - \rho_B(\mathbf{r})) \right] - \sum_{\alpha=1}^n \ln Q_\alpha[iw_A, iw_B; N_\alpha] \quad (S9) \end{aligned}$$

where $Q_\alpha[iw_A, iw_B; N_\alpha]$ is the single-chain partition function for α^{th} chain, given by

$$Q_\alpha = \frac{\int D[\vec{R}_\alpha] \exp\left\{-\frac{3}{2l^2} \int_0^{N_\alpha} ds \left(\frac{\partial \vec{R}_\alpha(s)}{\partial s}\right)^2 - \int_0^{N_{\alpha A}} ds iw_A(\vec{R}_\alpha(s)) - \int_{N_{\alpha A}}^{N_\alpha} ds iw_B(\vec{R}_\alpha(s))\right\}}{\int D[\vec{R}_\alpha] \exp\left\{-\frac{3}{2l^2} \int_0^{N_\alpha} ds \left(\frac{\partial \vec{R}_\alpha(s)}{\partial s}\right)^2\right\}} \quad (\text{S10})$$

The equation for Q_α is analogous to the Feynman-Kac formula in the path-integral description of quantum mechanics⁷ and may be expressed as

$$Q_\alpha = V^{-1} \int d\vec{r} q_\alpha(\vec{r}, N_\alpha) \quad (\text{S11})$$

where V is total volume and $q_\alpha(\vec{r}, s)$ is a restricted chain partition function that may be calculated as the solution to the modified diffusion equation

$$\frac{\partial q_\alpha(\vec{r}, s)}{\partial s} = \begin{cases} \frac{l^2}{6} \nabla^2 q_\alpha(\vec{r}, s) - iw_A(\vec{r}) q_\alpha(\vec{r}, s), & 0 < s < N_{\alpha A} \\ \frac{l^2}{6} \nabla^2 q_\alpha(\vec{r}, s) - iw_B(\vec{r}) q_\alpha(\vec{r}, s), & N_{\alpha A} < s < N_\alpha \end{cases} \quad (\text{S12})$$

subject to the initial condition $q_\alpha(\vec{r}, 0) = 1$.

Evaluation of discrete sum in Eq. S9 for polydisperse block copolymers is computationally extensive. In order to evaluate the sum, we approximate it by an integral over continuous chain length distribution as discussed in the next section.

Modeling polydispersity effects by continuous chain length distribution

In order to model di-block copolymers containing polydisperse A block and monodisperse B block, we assume that the A block has the chain-length distributed as per the *normalized* Schulz-Zimm

distribution^{1,8-10} given by

$$p_A(N) = \left(\frac{N}{N_A}\right)^{\nu-1} \frac{\exp[-N/N_A]}{N_A \Gamma(\nu)} \quad (\text{S13})$$

where ν and N_A control different properties of the distribution function. Also, Γ is the Gamma function. Assuming that the B block is monodisperse with fixed degree of polymerization ($= N_B$), the chain length distribution for the A-B di-block becomes $p_{AB}(N') = p_A(N')$ for $N' < (N - N_B)$ and $p_{AB}(N') = 0$ otherwise. Using the continuous chain length distribution, the discrete sum over chain index α in Eq. S9 can be replaced by integrals over chain lengths via $n^{-1} \sum_{\alpha=1}^n \ln Q_{\alpha}[i w_A, i w_B; N_{\alpha}] = \int_0^{\infty} dN p_{AB}(N) \ln Q[i w_A, i w_B; N]$.

The field theoretic transformations and approximation of continuous chain length distribution lead to deconvolution of chain-chain interactions into single chain problem, where each chain interacts with fields w_k . Even with these simplifications, numerical evaluation of the functional integrals in Eq. S8 poses a serious challenge. In the following, we approximate these integrals by saddle-point approximation so that the full partition function is approximated by its value when the fields attain their ‘‘saddle-point’’ values. Noting that the saddle-points are located along the imaginary axis in the complex- w plane,^{5,11} we rescale these fields by writing $\omega_A = i \langle N \rangle_n w_A$, $\omega_B = i \langle N \rangle_n w_B$, and $\eta = i \langle N \rangle_n p$ so that ω_A , ω_B and η are purely real and $\langle N \rangle_n = \nu N_A + N_B$ is the number average chain length for the di-block copolymers, assuming that the B block is monodisperse. Also, volume fractions are defined by $\phi_k(\vec{r}) = \rho_k(\vec{r}) / \hat{\rho}_0$ for $k = A, B, s, a$.

The value of the fields $[\phi_A, \phi_B, \omega_A, \omega_B, \eta]$ at the saddle-point satisfy the following set of equa-

tions

$$\omega_A(\vec{r}) = \chi_{AB} \langle N \rangle_n \phi_B(\vec{r}) + \sum_{k=s,a} \chi_{kA} \langle N \rangle_n \phi_k(\vec{r}) + \eta(\vec{r}) \quad (\text{S14})$$

$$\omega_B(\vec{r}) = \chi_{AB} \langle N \rangle_n \phi_A(\vec{r}) + \sum_{k=s,a} \chi_{kB} \langle N \rangle_n \phi_k(\vec{r}) + \eta(\vec{r}) \quad (\text{S15})$$

$$\phi_A(\vec{r}) + \phi_B(\vec{r}) = 1 - \sum_{k=s,a} \phi_k(\vec{r}) \quad (\text{S16})$$

$$\phi_A(\vec{r}) = \int_0^\infty dN \frac{P_{AB}(N)}{Q\{N/\langle N \rangle_n\}} \int_0^{(N-N_B)/\langle N \rangle_n} d\bar{s} q(\vec{r}, \bar{s}) q^\dagger(\vec{r}, \bar{s}) \quad (\text{S17})$$

$$\phi_B(\vec{r}) = \int_0^\infty dN \frac{P_{AB}(N)}{Q\{N/\langle N \rangle_n\}} \int_{(N-N_B)/\langle N \rangle_n}^{N/\langle N \rangle_n} d\bar{s} q(\vec{r}, \bar{s}) q^\dagger(\vec{r}, \bar{s}) \quad (\text{S18})$$

where

$$Q = V^{-1} \int d\vec{r} q(\vec{r}, N/\langle N \rangle_n) \quad (\text{S19})$$

and we have used $\rho_0 = n \langle N \rangle_n / V$ along with a well-known factorization of the single-chain path integral^{7,12,13} in writing Eqs. S17 and S18. Furthermore, solution to the restricted partition function q^\dagger , may be calculated as the solution to a modified diffusion equation similar to Eq. S12 subject to the initial condition $q^\dagger(\vec{r}, s = N/\langle N \rangle_n) = 1$.¹⁴

We have solved the set of equations representing saddle-point in the complex plane using an iterative procedure devised by Drolet and Fredrickson^{11,15} (so called ‘‘model A’’ type relaxation dynamics¹⁶). This results in the following expressions for updating the chemical potential fields from relaxation step n to $n + 1$

$$\begin{aligned} \omega_A^{n+1} - \omega_A^n &= \lambda' \frac{\delta \beta F}{\delta \phi_B^n} + \lambda \frac{\delta \beta F}{\delta \phi_A^n} \quad (\text{S20}) \\ &= \lambda' \left[\chi_{AB} \langle N \rangle_n \phi_A^n + \sum_{k=s,a} \chi_{kB} \langle N \rangle_n \phi_k - \omega_B^n + \eta^n \right] \\ &+ \lambda \left[\chi_{AB} \langle N \rangle_n \phi_B^n + \sum_{k=s,a} \chi_{kA} \langle N \rangle_n \phi_k - \omega_A^n + \eta^n \right] \end{aligned}$$

A similar equation is used for relaxing ω_B , and this is written as

$$\omega_B^{n+1} - \omega_B^n = \lambda \frac{\delta \beta F}{\delta \phi_B^n} + \lambda' \frac{\delta \beta F}{\delta \phi_A^n} \quad (\text{S21})$$

where the relaxation parameters are chosen such that $\lambda' < \lambda$ and $\lambda > 0$ and the quantities ϕ_A^n , ϕ_B^n are calculated as functionals of ω_A^n , ω_B^n using their expression in terms of q and q^\dagger . For the evaluation of integrals over the chain lengths in Eqs. S17 and S18, we have used the Gaussian quadrature scheme applied to the polydisperse di-block copolymer melts in Ref.⁹ For the results presented in this work, we have found ten quadrature points to be sufficient to provide converged results on the volume fraction profiles due to the fact that most of the calculations done in this work are in the weak segregation limit. For some of our test runs done in the intermediate and strong segregation, we have found that more quadrature points are required. The contribution of different quadrature points to the total volume fraction of the A monomers in a thin film of A-B di-block chains containing equal average volume fractions of the two blocks is shown in Figure S1.

The pressure field is updated using the expression

$$\eta^{n+1} = \frac{1}{2} \left[\omega_A^{n+1} + \omega_B^{n+1} - \chi_{AB} \langle N \rangle_n + (\chi_{AB} - \sum_{k=s,a} \{\chi_{kA} + \chi_{kB}\}) \langle N \rangle_n \phi_k \right] \quad (\text{S22})$$

After updating the pressure field, its spatial average $V^{-1} \int \eta(\vec{r}) d\vec{r}$ is subtracted so as to improve the algorithm's stability. This has no effect on the equilibrium structure of the chains as the thermodynamic properties are invariant to a constant shift in the pressure field. With the new fields ω_A , ω_B and η , the procedure is repeated until the saddle-point configurations are found.

Interpretation of neutron reflectivity profiles

As mentioned in the main text, for interpretation of neutron reflectivity profiles, we have followed a three step procedure. In the first step, an initial estimate of the film thickness was obtained using the spacing (in terms of momentum transfer vector q) between two fringes in the neutron reflectivity

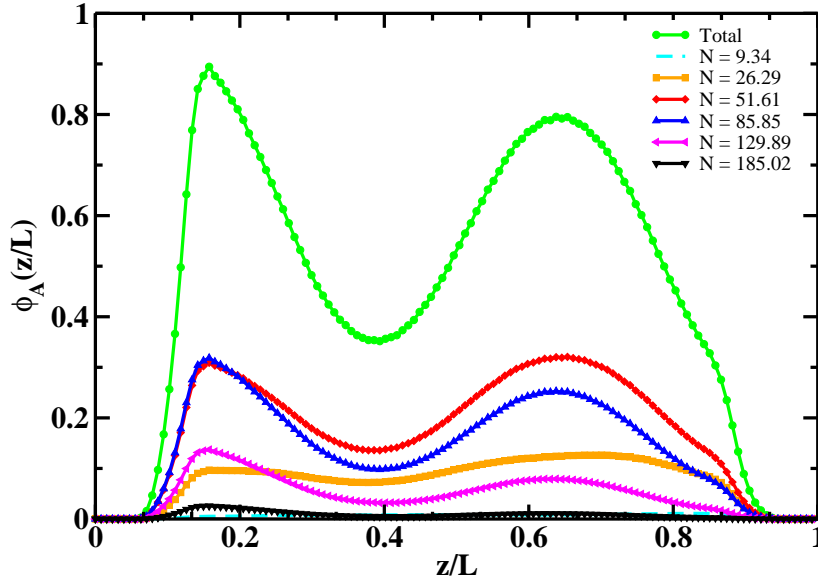


Figure S1: Contribution of different Gaussian quadrature points to the total volume fraction of the A monomers in a thin film of polydisperse A-B di-block copolymer chains containing equal average fraction of A and B block. “Total” corresponds to the sum of all of the ten quadrature points used for these calculations. These results were obtained by using $\chi_{AB} \langle N \rangle_n = 10$, $\chi_{sA} = \chi_{aB} = 0.001$, $\chi_{aA} = \chi_{sB} = 0.35$, $\text{PDI}_A = 1.36$ and a film of thickness $L = 5R_g$ in the SCFT.

data. With these film thicknesses, the SCFT simulations with the hyperbolic tangent masking functions (as discussed in the previous section) were used to determine the number of strata that are present in the thin film. These simulations were run to mimic the PGMA-PVDMA- d_6 systems with $\text{PDI}_{PGMA} = 1.36$ and different values of χ parameters characterizing monomer-monomer and monomer-substrate interactions. In the second step, a multi-layer model based on the number of strata and density profiles was constructed to fit the neutron reflectivity data using Parratt’s formalism.¹⁷ Predictions of the SCFT were used as an initial guess for the construction of multi-layer models, which makes it easier to find the best fit. Note that the SCFT provides description of density profiles at equilibrium in the thin films. However, it is not clear whether the multi-layer models corresponding to the best fits represent equilibrium or non-equilibrium structure due to the presence of kinetic effects in thin films. In order to distinguish between the two kinds of structures, we have taken a third step by extracting “refined” masking functions (see Figure S2) and total

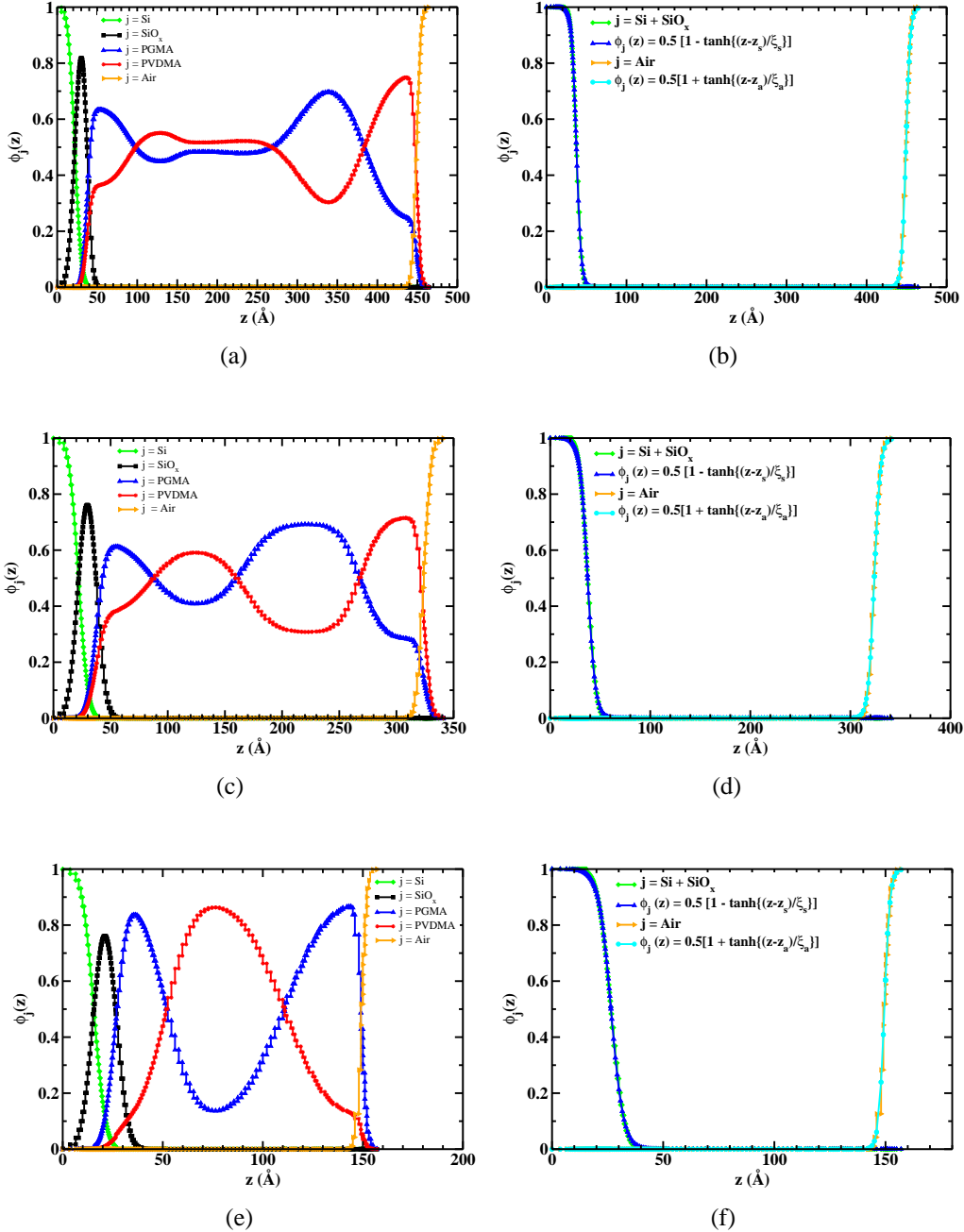


Figure S2: Extraction of masking functions from the multi-layer model corresponding to the best fit of neutron reflectivity profile for the three samples is described here. Figures (a),(c) and (e) show the volume fraction profiles of different components used in the multi-layer model. As the SCFT model doesn't distinguish between the silicon and its oxide layer, the masking function near these substrates represents the combined effects of these. In order to extract the masking functions, volume fractions of silicon and oxide layer on it are added, which is shown in Figures (b),(d) and (f); functions based on hyperbolic tangents are used to fit the volume fraction of air and silicon-silicon oxide layers. These masking functions are used to run the SCFT simulations with the different values of χ parameters.

film thicknesses from the best fits obtained using the two steps mentioned above and using these functions and thicknesses to run another round of SCFT simulations.

Table S2: Characteristics of extracted masking functions (given by Eqs. S3 and S4) from modeling of neutron reflectivity profiles.

	z_s (Å)	ξ_s (Å)	z_a (Å)	ξ_a (Å)
$L = 412.0$ Å	37.40	5.96	449.19	5.38
$L = 286.1$ Å	37.38	7.69	329.93	6.11
$L = 123.0$ Å	26.51	5.48	149.47	2.54

In order to obtain the volume fraction (ϕ_k) profiles from the SLD profiles of the best fits, we used the relation $SLD(\mathbf{r}) = \sum_{k=Air, Si, SiO_x, PGMA, PVDMA-d_6} SLD_k \phi_k(\mathbf{r})$, where SLD_k is the SLD and $\phi_k(\mathbf{r}) = m_k(\mathbf{r})/\rho_0$ so that ρ_0 is the reference mass density and m_k is the mass density of the component of type k . The SLD_k were computed using the molecular formula and the reference density ρ_0 . Furthermore, ρ_0 was varied to make sure that the spatial average of $\phi_k(\mathbf{r})$ is 0.5 for the three samples studied in this work. The volume fraction profiles for the silicon (ϕ_{Si}), silicon oxide (ϕ_{SiO_x}) and air (ϕ_{air}) were used to extract the masking functions for the SCFT simulations, as shown in Figure S2. In our SCFT model, the effects of silicon and silicon oxide layer appear through a single masking function that is given by Eq. S3 and effects of monomer-air are modeled by the masking function given as Eq. S4. In order to extract parameters z_s and ξ_s for the masking function that describes the silicon substrate, we have added the volume fractions of silicon and silicon oxide before fitting the profiles to Eq. S3. For the monomer-air interface, we have fitted the volume fraction of air to Eq. S4. The fits are shown in Figure S2 for the three films studied in this work and the fit parameters are presented in Table S2.

Volume fraction profiles for the PGMA and PVDMA-d₆, obtained from the SLDs representing the best fits for the neutron reflectivity data are compared with the profiles obtained from the SCFT simulations. Different SCFT results were obtained for the volume fraction profiles inside the film by varying five χ parameters. For setting up dimensionless parameters mimicking the three films, we have estimated $R_g = (\langle N \rangle_n l^2 / 6)^{1/2} = 39.6$ Å, corresponding to $\langle N \rangle_n = 284$ (instead of 290, which preserves equal fractions of PGMA and PVDMA-d₆) obtained from molecular characteri-

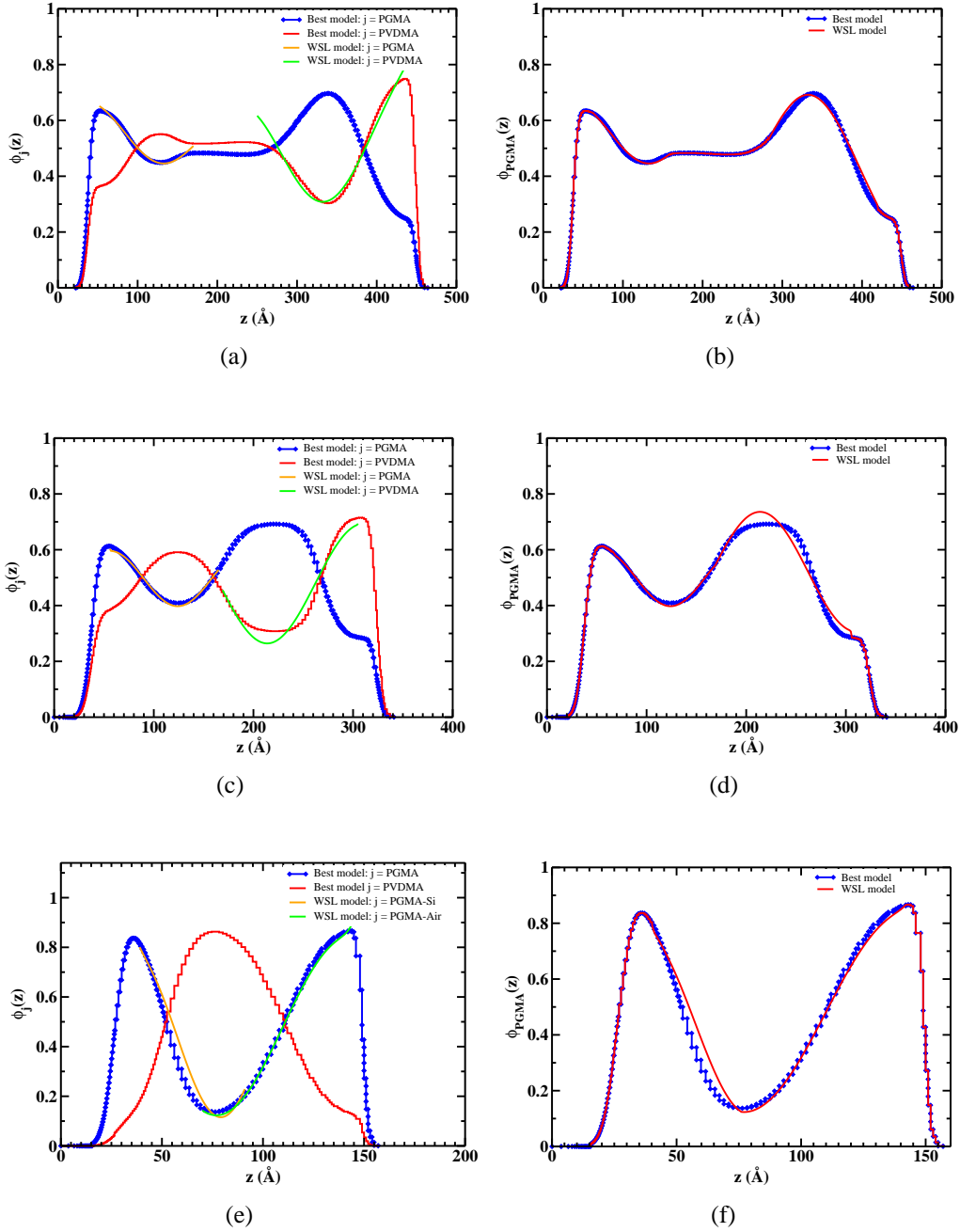


Figure S3: Procedure for extracting the $\chi \langle N \rangle_n = \chi_{PGMA-PVDMA-d_6} \langle N \rangle_n$ from the volume fraction profiles corresponding to best fits of neutron reflectivity profiles for the three films studied in this work. Left figures show *independent* fits to the volume fraction profiles near each substrate using Eq. S23. Right figures show the volume fraction profiles after the addition of masking functions. For the thickest films, flat region in the interior of the film can not be modeled by the analytical profiles and the region is kept the same in obtaining the figure on the right hand side.

zation of the PGMA-PVDMA- d_6 di-block copolymers presented in Table 1 in the main text and $l = \sqrt{l_{PGMA}l_{PVDMA-d_6}} = 5.75 \text{ \AA}$, which is estimated using group contribution method (cf. Table S1). Due to the fact that each SCFT calculation is computationally extensive and takes around four hours to obtain converged density profiles on eight cores in parallel execution, it is not practical to vary the five χ parameters in an arbitrary fashion. As it turns out, the polydisperse di-blocks studied in this work lie in the weak and intermediate segregation limit. So, we have estimated the χ parameters using an analytical theory applicable in the weak segregation limit¹⁸ (WSL). The theory is a straightforward generalization from the case of monodisperse to polydisperse copolymers. Details of the theory will be presented elsewhere. Volume fraction profiles obtained from the modeling of neutron reflectivity data can be readily fit with the predicted functional form in the so-called “ordered bulk” regime, in the parlance of Ref.¹⁸ and written as

$$\phi_j(z) = f_j + \sqrt{\frac{8\bar{\chi}\varepsilon}{\Delta}} E(z - z_0) \cos[q_0(z - z_0) + \phi] \quad (\text{S23})$$

$$E(z) = \frac{1 - \mu(\phi) \exp\left[-\sqrt{2}z/\xi_-\right]}{1 + \mu(\phi) \exp\left[-\sqrt{2}z/\xi_-\right]} \quad (\text{S24})$$

$$\mu(\phi) = \frac{1 - q_1(\phi)}{1 + q_1(\phi)} \quad (\text{S25})$$

$$q_1(\phi) = \left[\frac{\xi_-^2}{2} \left(q_0 \tan \phi + \frac{1}{\lambda} \right)^2 + \frac{H_1 \xi_-}{B \cos \phi} \sqrt{\frac{\Delta}{4\bar{\chi}\varepsilon} + 1} \right]^{1/2} - \frac{\xi_-}{\sqrt{2}} \left[q_0 \tan \phi + \frac{1}{\lambda} \right] \quad (\text{S26})$$

The parameter H_1 characterizes the difference in the chemical potential between PGMA and PVDMA- d_6 to be at different surfaces. In the SCFT, this is equivalent to the difference in χ_{jPGMA} and $\chi_{jPVDMA-d_6}$ so that $j = s, a$. $\varepsilon = (\chi - \chi_s)/\chi_s = 2/(q_0^2 \xi_-^2)$, so that χ_s is the value of $\chi = \chi_{PGMA, PVDMA-d_6}$ at the stability limit of the disordered phase. For the physical interpretation of other parameters appearing in Eq. S23, the interested reader should refer to Ref.¹⁸ For estimating the χ parameters using Eq. S23, we have set $\lambda \rightarrow \infty$, which, in turn, corresponds to setting the “extrapolation length” a_1 in Ref.¹⁸ to zero. We have done this by keeping in mind the fact that the Hamiltonian used for the construction of the SCFT doesn’t have a term dependent on the “extrap-

olation length” a_1 in the surface free energy density. For these fits, each substrate is assumed to behave independent of each other. As the analytical theory doesn’t take into account the depletion zone, we have used z_0 as the starting point for the fitting and index j corresponds to the component near each wall. $H_1/B, \tan \phi, \xi_-, q_0^{-1}$ and $\sqrt{(4\bar{\chi}\epsilon)/\Delta}$ are taken as the fit parameters, which are shown in Table S3 for the silicon and air sides.

Table S3: Parameters obtained by fitting volume fraction profiles using Eq. S23

	Silicon side $L = 412.0 \text{ \AA}$	Air side $L = 412.0 \text{ \AA}$	Silicon side $L = 286.1 \text{ \AA}$	Air side $L = 286.1 \text{ \AA}$	Silicon side $L = 123.0 \text{ \AA}$	Air side $L = 123.0 \text{ \AA}$
H_1/B	1.32×10^{-3}	1.75×10^{-3}	3.33×10^{-4}	5.93×10^{-11}	2.37×10^{-3}	1.54×10^{-3}
$\tan \phi$	-1.13×10^{-3}	-3.21×10^{-7}	-8.19×10^{-11}	-2.16×10^{-1}	-3.18×10^{-8}	-6.70×10^{-3}
ξ_-	3.06×10^3	3.06×10^3	1.46×10^2	1.51×10^2	4.00×10^1	6.35×10^1
q_0^{-1}	2.53×10^1	3.28×10^1	2.15×10^1	3.13×10^1	1.36×10^1	2.11×10^1
$\left[\frac{4\bar{\chi}\epsilon}{\Delta}\right]^{1/2}$	1.92×10^{-3}	7.42×10^{-3}	5.66×10^{-2}	1.00×10^{-1}	2.17×10^{-1}	2.32×10^{-1}
$\chi \langle N \rangle_n$	9.17	9.17	9.56	9.96	11.29	11.20

The fits are shown in Figure S3. From the fit parameters shown in Table S3, $\chi = \chi_{PGMA-PVDMA-d_6} \langle N \rangle_n$ is computed using the relation $(\chi - \chi_s)/\chi_s = 2/(q_0^2 \xi_-^2)$. $\chi_s \langle N \rangle_n$ and the characteristic length scale appearing at the stability limit of disordered phase in the polydisperse case have already been presented in the literature and we have reproduced those results, as shown in Figure S4. In the process, we have found typographical errors in Eqs. (37) and (38) of Ref.,⁹ which are relevant for the computation of stability limit of the disordered phase. In particular, the Eqs. (37) and (38) in that work should read as

$$S_{BB}^o(q) = \frac{2N_n}{x^2} \left[\left\{ 1 + \frac{N_b x}{N_n} \right\}^{-\alpha} - 1 + \frac{\alpha N_b x}{N_n} \right] \quad (\text{S27})$$

$$S_{AB}^o(q) = \frac{N_n}{x^2} \left[\exp \left\{ -\frac{N_A x}{N_n} \right\} - 1 \right] \left[\left\{ 1 + \frac{N_b x}{N_n} \right\}^{-\alpha} - 1 \right] \quad (\text{S28})$$

where $x = q^2 N_n b^2 / 6$. Here, we have used the same notation as in Ref.⁹

Note that we have used the assumption that volume fraction profile near each substrate is not affected by the presence of the other substrate. Such an assumption facilitates the fitting and, at the same time, provides useful information regarding the confinement effects. For example, the esti-

mated values of $\chi_{PGMA-PVDMA-d_6} \langle N \rangle_n$ based on this assumption are equal for the two substrates in the case of the thickest film (i.e., $L = 412.0 \text{ \AA}$) studied in this work. However, for the thinner films, values of $\chi_{PGMA-PVDMA-d_6} \langle N \rangle_n$ determined from the fitting of volume fraction profiles near each substrate differ from each other and reveals the presence of confinement effects. Nevertheless, these estimates provide a useful range of $\chi_{PGMA-PVDMA-d_6} \langle N \rangle_n$, which we have used in the numerical SCFT and computed the volume fraction profiles in films containing polydisperse di-block copolymers.

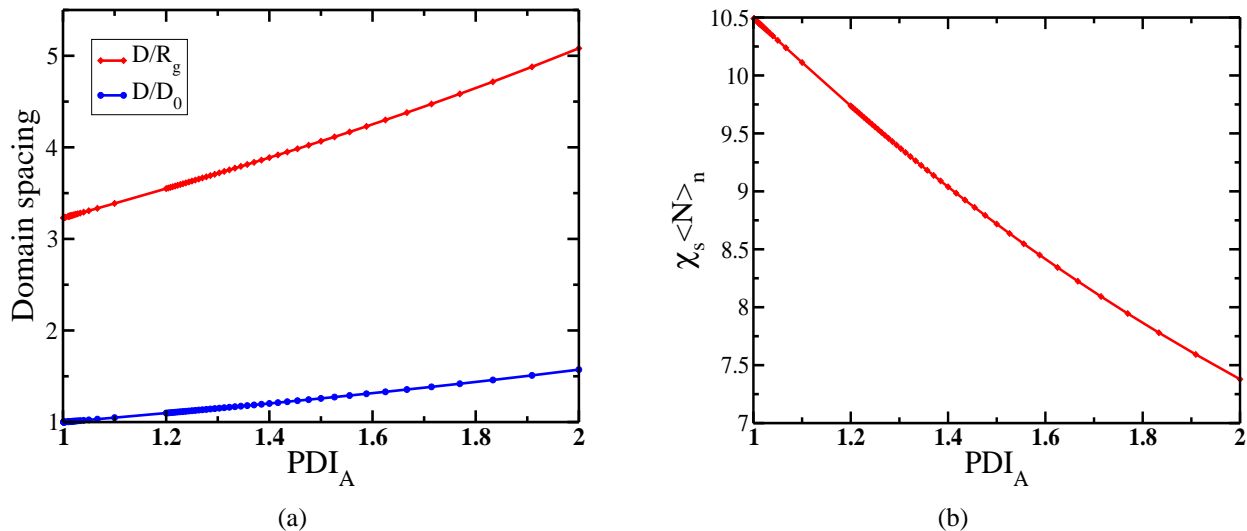


Figure S4: Characteristics of the domain spacing ($D = 2\pi/q^*$, q^* being the wave-vector at the minimum of the free energy at the stability limit) and $\chi_s \langle N \rangle_n$ in the polydisperse A-B di-block copolymers as predicted by the weak segregation theory. D_0 is the domain spacing at the stability limit of monodisperse di-block copolymer melts. The di-block copolymers contains equal average volume fractions of A and B monomers.

References

- (1) Flory, P. *Principles of Polymer Chemistry*; Oxford University Press: Ithaca, 1953.
- (2) Doi, M.; Edwards, S. F. *The Theory of Polymer Dynamics*; Clarendon Press: Oxford, 1986.
- (3) van Krevelen, *Properties of Polymers*; Elsevier, 1990.

- (4) Wu, D.; Fredrickson, G.; Carton, J.; Ajdari, A.; Leibler, L. *Journal of Polymer Science: Part B: Polymer Physics* **1995**, *33*, 2373–2389.
- (5) Fredrickson, G. *The Equilibrium Theory of Inhomogeneous Polymers*; Clarendon Press: Oxford, 2006.
- (6) Matsen, M. W. *Journal of Chemical Physics* **1997**, *106*, 7781–7791.
- (7) Feynman, R. P.; Hibbs, A. R. *Quantum Mechanics and Path Integrals*; McGraw-Hill Book Company: New York, 1965.
- (8) Fredrickson, G. H.; Sides, S. W. *Macromolecules* **2003**, *36*, 5415–5423.
- (9) Sides, S. W.; Fredrickson, G. H. *Journal of Chemical Physics* **2004**, *121*, 4974–4986.
- (10) Lynd, N. A.; Meuler, A. J.; Hillmyer, M. A. *Progress in Polymer Science* **2008**, *33*, 875–893.
- (11) Fredrickson, G. H.; Ganesan, V.; Drolet, F. *Macromolecules* **2002**, *35*, 16–39.
- (12) Freed, K. F. *Adv. Chem. Phys.* **1972**, *22*, 1.
- (13) Helfand, E. *J. Chem. Phys.* **1974**, *62*, 999–1005.
- (14) Matsen, M. W.; Schick, M. *Phys. Rev. Lett.* **1994**, *72*, 2660–2663.
- (15) Drolet, F.; Fredrickson, G. H. *Phys. Rev. Lett.* **1999**, *83*, 4317–4320.
- (16) Hohenberg, P. C.; Halperin, B. I. *Rev. Mod. Phys.* **1977**, *49*, 436–475.
- (17) Parratt, L. G. *Physical Review* **1954**, *95*, 359–369.
- (18) Fredrickson, G. H. *Macromolecules* **1987**, *20*, 2535–2542.